Structures 48 (2023) 736–753

Contents lists available at ScienceDirect

Structures

journal homepage: www.elsevier.com/locate/structures

Bending performance of dapped-end beams having web opening: Experimental and numerical investigation

Ceyhun Aksoylu [a], Yasin Onuralp Özkılıç [b,*], Emrullah Çeledir [a], Musa Hakan Arslan [a]

[a] Faculty of Engineering and Natural Sciences, Department of Civil Engineering, Konya Technical University, Konya 42130, Turkey
[b] Faculty of Engineering, Department of Civil Engineering, Necmettin Erbakan University, Konya 42000, Turkey

ARTICLE INFO

Keywords:
Bending
Beam
Purlin
Dapped-end beam
Opening
Experimental analysis
Numerical analysis

ABSTRACT

Reinforced concrete dapped-end (purlin) beams are frequently used in prefabricated industrial structures. The main task of these beams is to safely carry the loads on the roof. Considering the number of these purlin beams in industrial buildings, it is extremely important for manufacturers to product these beams with less concrete without reducing the load carrying capacity. Since these purlin beams are under the effect of bending and shear forces, controlled creating openings in beam span can have significant economic benefits for the manufacturer. Therefore especially economic design perspective, it is so crucial to determine the amount of openings that will not cause a significant change in the bending behavior. In this study, the behavior of dapped-end purlins with openings was experimentally and numerically investigated. In the experimental step, seven purlin beams having different opening configurations were tested under four-point loading to investigate the openings effects on beam structural behavior. In this step opening length to total length varying between 0.075 and 0.325 was selected as a main parameter. After test, the numerical models were created and verified using experimental findings. After this step, in the parametric study part of the paper, the effects of shear span, depth of the opening and length of opening and different opening configurations (such as segmentation) which were not tested in experiments, were examined. The experimental outcomes revealed that increases in the opening did not provide a significant effect on the load capacity. This can be explained by the fact that the openings are in the bending region. The numerical findings showed that increasing shear span to depth ratio (a_v/d) ratio did not change rigidity but decreased the load capacity. However, no effect was observed on the opening height provided that it is at least as far away from the upper and lower longitudinal reinforcements bars as the concrete-cover margin. On the other hand, increasing opening/purlin length (especially higher than 0.375) reduces the capacity. However, segmented openings (multiple openings instead of single whole openings) did not reduce capacity even if total opening/purlin length was 0.525.

1. Introduction

Reinforced concrete prefabricated structures are preferred especially in large-span industrial structures because they are more economical than other construction methods (conventional, steel, etc.). Rapid production of prefabricated reinforced concrete structures, high material quality, modularity and disassembly are important advantages [1–5]. However, the biggest problem of the structures produced with concrete is the increasing demand for raw materials in the world in recent years, and the price increase due to the gradual decrease of natural resources [6–13]. In addition, the damage caused by cement and aggregate production to the environment is an important issue that is highly debated [14–17]. For this reason, economic improvements to be made in the sections of reinforced concrete structures, the most important of which is the reduction of the concrete raw material used, is of great importance in the global environment.

Although it is thought that one of the most effective ways in the economical design of reinforced concrete sections is to increase the strength of the material used and to reduce their cross-section, deflection problems under vertical loads often do not make this possible in terms of usage limits in especially wide-span beams and slabs. Similarly, the concern of sufficient horizontal stiffness in columns, especially under the effect of earthquakes, is a compelling factor for the column inertia to remain above a certain level. For this reason, designers want to reduce

* Corresponding author.
E-mail address: yozkilic@erbakan.edu.tr (Y.O. Özkılıç).

https://doi.org/10.1016/j.istruc.2022.12.110
Received 9 August 2022; Received in revised form 25 November 2022; Accepted 28 December 2022
Available online 5 January 2023

Fig. 1a. Prefabricated reinforced concrete hollow slab

Fig. 1b. Prefabricated reinforced concrete hollow rafters

Fig. 1. Openings created in prefabricated floor and roof beams.

Fig. 2a. Simple-scale industrial structures

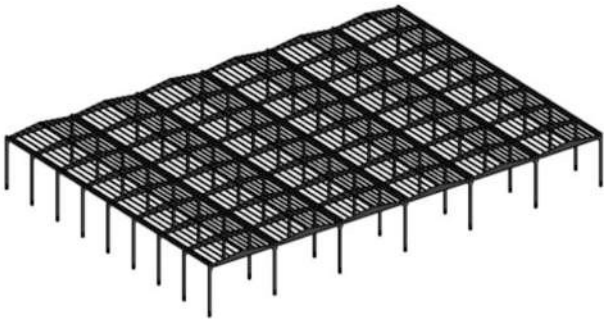

Fig. 2b. Large-scale industrial structures

Fig. 2. Purlin quantities used in simple and large-scale industrial structures.

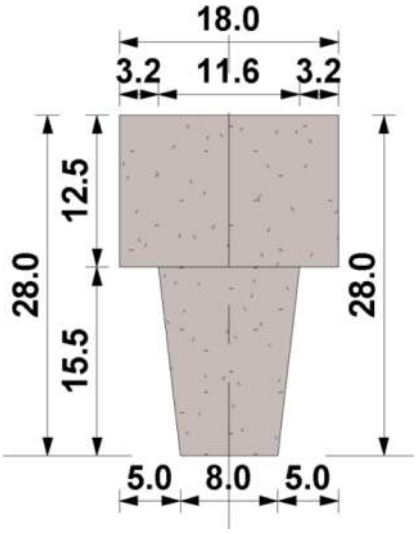

Fig. 3. Cross-sectional properties of the reference purlin beams (P-0).

concrete consumption to some extent by creating openings in reinforced concrete elements where the bearing capacity and inertia of the section are not needed much. Especially in beams under moment and shear forces, these arrangements can be made more easily. Appropriate narrowing or creating openings (gaps) in sections (under the supervision of the designer and designed) in areas where the moment is effective can give appropriate results without changing the bearing capacity and rigidity of the section [18,19,54].

However, it has been stated in many studies in the literature that the openings, which are mostly opened in an unplanned manner and formed in the regions close to the support, cause a great decrease in the capacity due to the reduction of the shearing capacity of the section. Experimental studies on deep beams [20–23,52,53] and slender beams [24] were emphasized. It has been mentioned in the literature that it is necessary to strengthen the section with an appropriate method (FRP, steel wrap, etc.) [25], especially in order to eliminate the capacity loss caused by the opening. In these studies, researches were also carried out according to the geometry of the gap to be opened (circular, rectangular, etc.) and the additional reinforcement arrangements around the gap [26–29].

Especially in prefabricated reinforced concrete structures, it is thought that the openings that will be created in the factory environment in the appropriate parts of the bending elements (beams, flooring, etc.) will have significant returns in large-scale productions. For this reason, prefabricated building manufacturers have made economic approaches by reducing the sections in the main roof beams and slabs of the industrial structure, in the sections that are effective for bending, and in the regions close to the neutral axis where the stress is close to zero (Fig. 1a and 1b). The relatively limited span (5–8 m) of the slab in Fig. 1a has made the use of hollow floors extremely common. However, as shown in Fig. 1b, its application is limited due to the gap left in the rafters, the difficulty of manufacturing, and the formation of compression and tension cracks at the joint points of the roof beams, especially with large spans (15–25 m).

There is no research about openings in the literature on purlin beams, which are other important members of prefabricated buildings. Although there are studies that include improvements on the dapped ends of purlins, which are particularly critical points [30–32], economical section design is an important gap in the literature. The rate at which purlins affect the total cost of industrial buildings is variable. For example, in a very small industrial structure (Fig. 2a), it is seen that the concrete used in the purlins constitutes 18 % of the concrete consumption in the building, while the share of the purlins in the total concrete quantity can increase up to 35 % as the area of the facility increases (Fig. 2b). This shows that limiting the use of concrete in purlin elements in industrial facilities will have significant benefits in every respect.

As stated above numerous studies have been conducted on beams having different openings in the literature. There are basically-two

Table 1
Designed purlins.

Specimen	Cross section (d = 26.5 cm, a_v = 95 cm, L = 320 cm, a_v/d = 3.58)	Opening Size (cmxcm)	Opening/Total Length Ratio
P-0	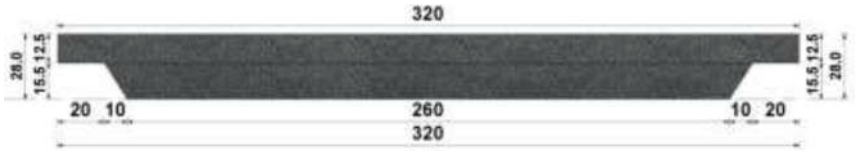	–	–/–
P-1	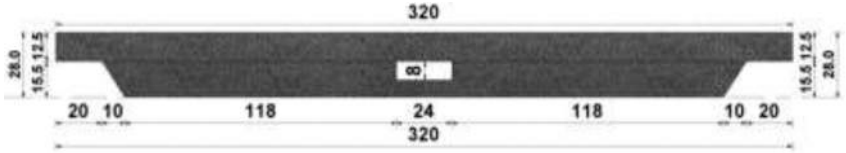	24 × 8	0.075
P-2	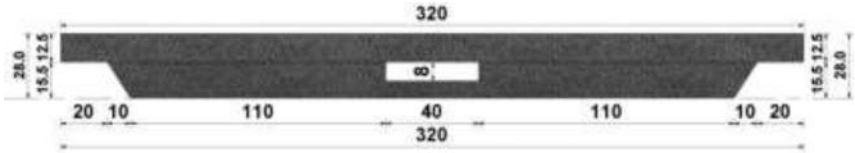	40 × 8	0.125
P-3	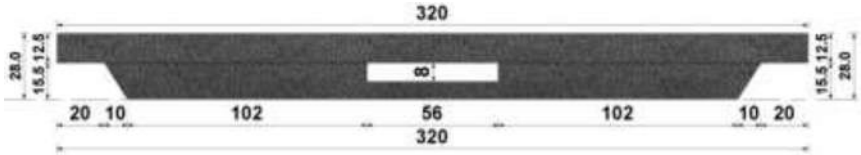	56 × 8	0.175
P-4	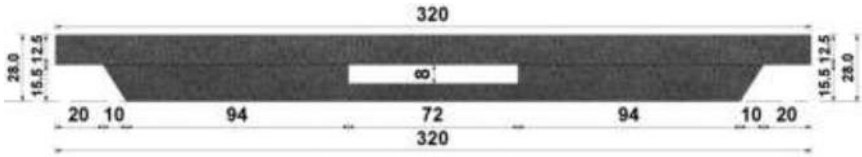	72 × 8	0.225
P-5	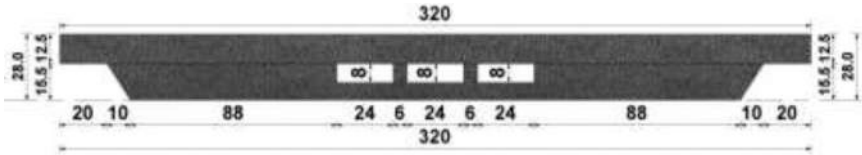	3x24x8	0.225
P-6	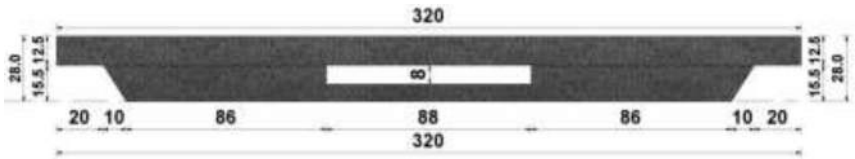	88x8	0.275
P-7	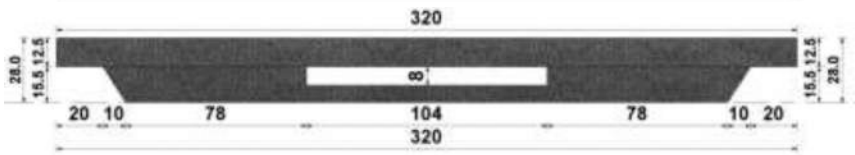	104x8	0.325

different situations in these studies. First situation; it is the case that the openings are drilled after the production of the beam. This situation is frequently encountered especially in basement floor beams when the installation gaps are passed through the beams. Therefore, in these studies, openings (generally circular holes) were chosen close to the support area (within the shear opening) [26,33–35]. The second situation is that the spaces are planned in a controlled manner during beam production (cast in place opening). In this case, some measures are taken to prevent damage around the openings. For example, additional reinforcements are suggested around the openings [35]. In addition to this situation, in the literature different opening geometry (such as circular, rectangular, triangular etc.) margins have been considered [36,37]. However, in the important part of the studies, the circularity of the spaces was studied.

The motivation of this study is quite different from the situations summarized above. First of all, the selected beams are geometrically and statically different from other beams. In addition, the reason for creating an opening is to make the beams lighter. Because the lightness of these beams on the roof of an industrial building will not only reduce the use of materials (especially concrete), but also reduce the inertial forces that will occur during an earthquake. For testing optimum amount of the openings, the gaps were increased gradually in this study. The test series was terminated as soon as there was a considerable reduction in the load carrying capacity. The main difference is that the spaces are chosen as rectangular and segmented rectangles, unlike the literature. While the behavior in the shear zone has been investigated in the literature, in this study, openings were created in the bending zone as it was aimed to lighten the beams. In this way, for purlins, especially for manufacturers,

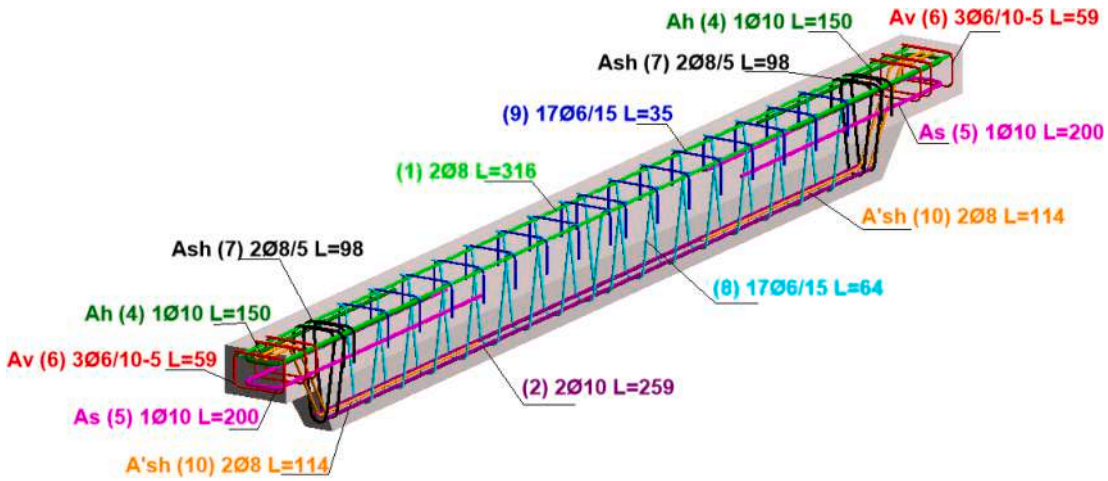

Fig. 4. Reinforcement details of the purlins.

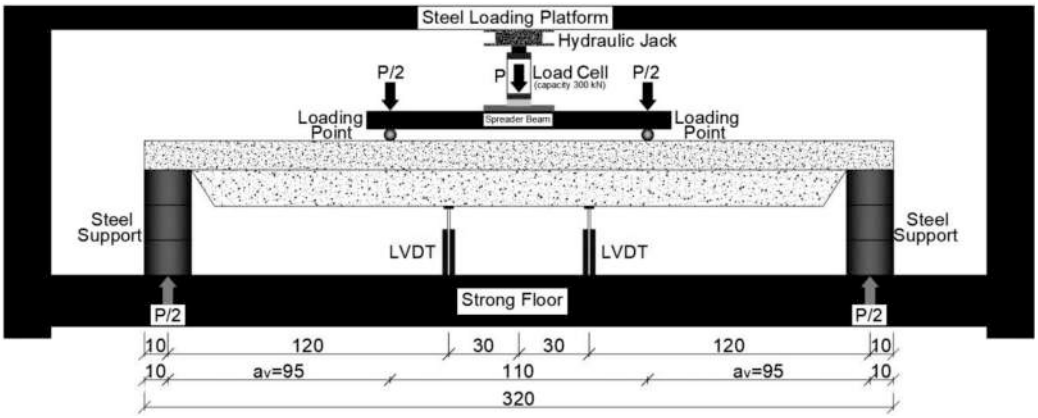

Fig. 5. Four-point bending test setup.

which void ratio will not affect the purlin behavior, in other words, the boundary condition in the void has been determined.

In prefabricated buildings, purlins are connected to the roof supports by means of steel pins due to the structure of the carrier system. They transfer the snow, wind, coating loads on the roof and the distributed load consisting of their own weight to the beam supports. For this reason, purlins have positive moments only in their openings, and the shear force effects are greater in the support regions. In this respect, it may be possible to narrow it (or manufacture it with a cavity) closer to the neutral axis region in opening sections where bending is more effective in purlin sections. But the determination of the gap width is an important issue.

In this study, openings were formed in the middle section of the bending effect region of 320 cm length purlins produced in full sectional scale (1/1). The openings are same height of 8 cm and varying lengths (24, 40, 56, 72, 3x24, 88 and 104 cm). The changes in the load carrying capacity, ductility and energy absorption capacities of purlins of a total of seven different sizes of openings were experimentally investigated. For this purpose, a total of 8 purlins, one of which is without an openings (reference), were subjected to bending tests at four points. The ratio of shear span to effective depth (a_v/d) for bending damage was chosen to be 3.58. Experimental load–displacement curves and progressive damages types obtained from the study were also obtained with the ABAQUS finite element program for similar load, support and material conditions. After the verification of the experimental study with numerical modeling, a parametric study was carried out by creating purlin models that were not tested in the experiments. In the parametric study, the results were generalized by considering three different (a_v/d), three different depth of openings and three different lengths of openings. In addition, in order to compare the behavior of the specimen with 3 × 24 (72 cm) segmented openings, the case of three different segmented opening widths is also considered.

2. Experimental program

2.1. Test specimen details and preparation

1/1 full scale dapped ended purlin beams with openings were produced in a prefab firm. One of these beams is a reference (without opening) and the other seven purlins consists different opening sizes. The lengths of the dapped ended beams were designed as 320 cm. Expanded Polystyrene Rigid Foam (EPS-26 kg/m^3 density) was used to create a void in the beams body. Rectangular spaces are formed in the beam bending zone at the center of the body and extending down from the upper head at a fixed height of 8 cm and a length of 24, 40, 56, 72, 3 × 24, 88 and 104 cm, respectively.

The geometric features of the cross-sections of the reference beam with no openings in its body and the beams with an opening are shown in Fig. 3 and the length sections are shown in Table 1. In Table 1, it was ensured that the beams reached their maximum load carrying capacity with bending damage according to these different opening areas. In addition, the effect of the opening space on the load bearing capacity and ductility of the beam can be examined, since the increasing gap length (space increase) in the horizontal direction of beams with a fixed

Fig. 6. Test specimens.

height of 8 cm changes with the length of the beam (320 cm). Here, since the top chord area is larger than the bottom chord area, the behavior change under load is investigated.

The average cylinder concrete compressive strength and splitting tensile strength (splitting) of purlins were obtained as 39.7 MPa and 2.55 MPa, respectively, as a result of 3 cube (cylinder equivalent) and 3 cylinder tests performed in the laboratory. According to TS 9967 [38] and Concrete Prefabrication Handbook [39],the production was carried out considering 2 pieces of Φ8 suspension reinforcement (A_{sh}) and the length of the tension reinforcement in the thinned region was 1.7 l_b (476 mm, l_b is embedment length). Therefore, the longitudinal reinforcement B420c type 2Φ10 and 2Φ8 were considered in the tensile and compressive regions of each beam, respectively. In addition, 3Φ6 suspension reinforcements (A_v), 1Φ10 shear friction reinforcement (A_h) and 1 U-shaped tensile reinforcement (A_s) in the thinned region, 2Φ8 suspension reinforcements (A_{sh}) and 2Φ8 Z type reinforcements. In addition, Z type reinforcement is a new type of reinforcement detail that increases the shear capacity recommended in the study of Aksoylu et al. [32]. The mechanical properties of the reinforcements in the study were taken into account in the previous study by the authors [40]. Fig. 4 shows the purlin beam reinforcement details tested in the experiments.

2.2. Test set up

The experimental setup used for the tests under vertical load of thinned-ended purlin beams with an opening is shown in Fig. 5. Four-point bending tests of beams under vertical load were performed by taking the shear span/effective height ratio (a_v/d) 3.58 to observe bending damage in beams. Two LVDTs were placed 60 cm apart to perform displacement measurements under vertical load. With the hydraulic piston in the experimental setup, the load was first applied to the simply supported spreader beam, and then the reactions of this beam were transferred to the reinforced concrete beam. The magnitude of the applied load during the experiment was measured with a load cell with a capacity of 300 kN. Loads were applied to the beams in 10 kN increments until the moment of yielding (M_r), and after the yielding was

Fig. 7. Damage history of P-0.

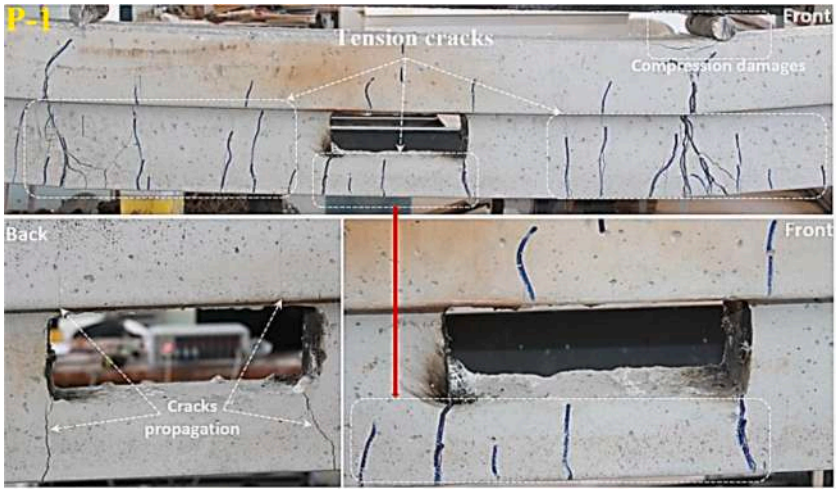

Fig. 8. Damage analysis of P-1.

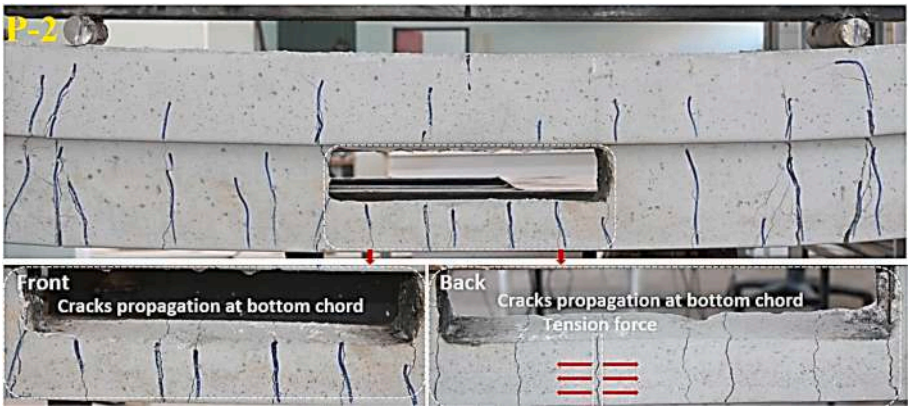

Fig. 9. Damage analysis of P-2.

observed on the load–displacement curve, the displacement-controlled loading was continued until the failure was reached. The bending cracks formed in the beams during the experiment were marked. Fig. 6 shows the reference beam and the pre-experimental layout of purlins.

Fig. 10. Damage analysis of P-3.

Fig. 11. Damage analysis of P-4.

3. Discussion of test results

3.1. Experimental test results

In the experimental study, the P-0 reference (without opening) beam was first tested. The first cracks in the P-0 beam were observed at the load level of 30 kN in the tension region. As the load reached 40 kN, the number of cracks in the tensile zone increased and the crack elongation proceeded towards the beam flange. With the vertical load of 47.6 kN and the current displacement of 11.1 mm, yielding occurred. After this stage, displacement controlled loading was started. The displacement increments were applied as 10 mm. With the increasing displacements, both new cracks started to form and the loading continued until the 62 mm displacement was reached as the cracks in the tension zone continued to expand. The experiment was terminated at this displacement value in order to prevent any deterioration in the experimental setup. At the end of the experiment, no damage was observed in the shear zone and supports of the beam, and the beam reached its bending capacity and exhibited ductile behavior. The first cracks (1), elastic cracks up to the yield point (2), cracks at the yield point (3), the damage condition at the end of the test (4) of P-0 specimen are shown in Fig. 7.

The first cracks on P-1 - P-7 beams were observed at a 67 % lower load level (10kN) compared to P-0. Therefore, the gaps opened in the bending region of the beams have led to a decrease in the bending stiffness of the beams within the elastic limits. When the P-1 beam reaches a load level of 52 kN and a displacement of 12.2 mm, it begins to yield. After this stage, displacement-controlled loading was continued with 10 mm increments until the end of the test displacement of 50.2 mm. An increase of 5.4 % and 9.9 %, respectively, was observed in the load and displacement values at the time of yield of P-1 compared to P-0. This situation led to an increase in vertical displacement as a result of the decrease in bending stiffness of the section (P-1) with decreasing

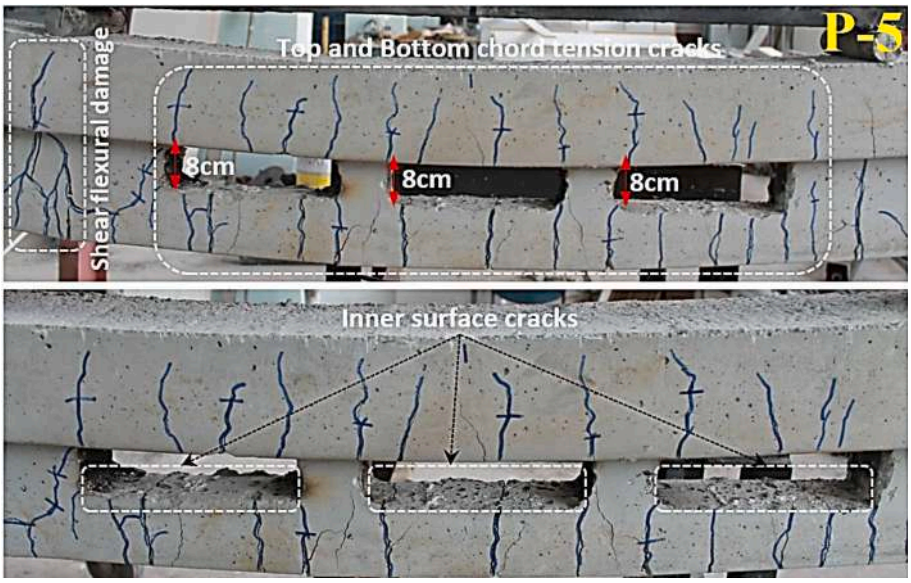

Fig. 12. Damage analysis of P-5.

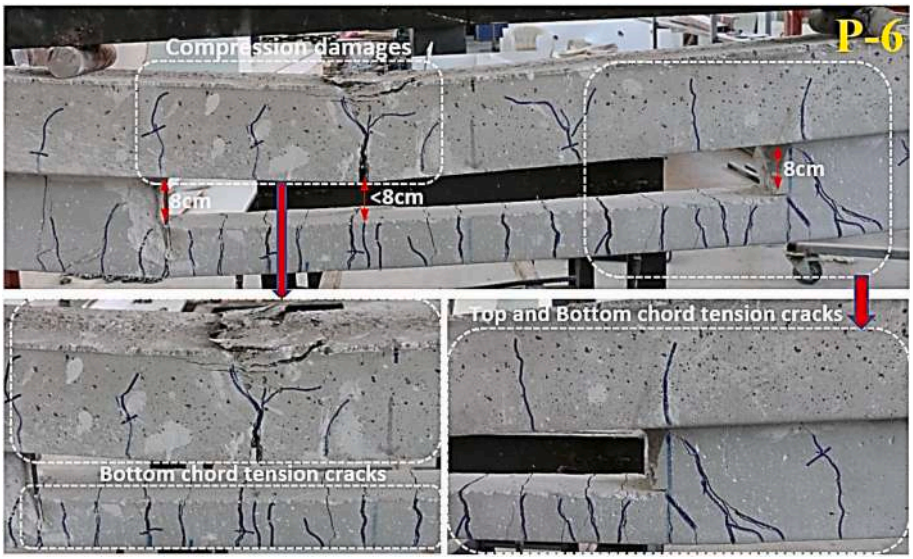

Fig. 13. Damage analysis of P-6.

moment of inertia. Damages in P-1 are shown in Fig. 8. Bending damages in P-1 occurred similarly to P-0. However, the damage was observed not only between the loading points under the spreader beam, but also in shear area. Crack propagation has been observed especially due to stress concentrations around the opening. In addition, crack widths under the loading points increased and more damage was observed in the bottom chord under the opening in the beam center (Fig. 8). Finally, with the beam reaching its bending capacity, crushing occurred below the spreader beam's right support loading point in the beam compression region (Fig. 8).

As soon as the P-2 reached a load of 47 kN and a displacement of 13 mm, it started to yield. The yield moment for P-2 occurred at the same load level as for P-0. However, the displacement value of P-2 at the time of yield was 17 % higher than P-0 and 6.5 % higher than P-1. This situation caused the stiffness value of P-2 to decrease by 17 % compared to P-0. At the end of the experiment, the damages in P-2 are quite similar to P-1. The damage to the P-2 is concentrated in the bending zone and the support points under the spreader beam. However, more cracks occurred in the bottom chord as opening area increased in the P-2 (Fig. 9).

The opening area created in the P-3 was 133 % (2.33 times) compared to P-1 and 40 % (1.44 times) more than P-2 (Fig. 10). This resulted in an increase of 29 % and 10 %of the displacement value at the time of yield of P-3 compared to P-1 and P-2, respectively. It also caused a 14 % decrease in the stiffness value of P-3 at yielding compared to P-0. The damages occurred in P-3 at the end of the experiment are quite similar to P-1 and P-2. However, the increase in the void area accelerated the pressure damage at the support points under the spreader beam. Cracks formed under the left support of the spreader beam towards the end of the test draw attention as shear bending cracks. In other words, the increase in the opening has led to a change in the location of the damage. In addition, since the cross-sectional area of the bottom chord decreases, the damages are concentrated around the opening with the increase in tensile stresses. Since the cross-sectional area of the beam in the compression region (top chord) is larger, the stresses are observed less and the crack density is also lower (Fig. 10).

Fig. 14. Damage analysis of P-7.

For beam P-4, when the load reached 10 kN, vertical cracks initiated in the concrete below the web opening, and these cracks were known as "elastic cracks". As the load increased 40.3 kN (in other words, the loads reached 50.3 kN), bending cracks initiated from the web opening top chord and propagated towards the spreader beam supports on the left and right side; these cracks were known as "plastic cracks". The opening area created in the P-4 is 200 % (3 times) more than P-1, 80 % (1.8 times) compared to P-2 and 28.5 % (1.28 times) more than P-3. This resulted in an increase of 37 %, 24.5 %, 16.9 % and 6.2 % of the displacement value of P-4 of yielding stage compared to P-0, P-1, P-2 and P-3, respectively. As the opening area increased, more cracks occurred in the bottom chord. In addition, the gap height decreased with the increase of the load. This situation was caused by the deterioration of the stability of the bottom chord and the crushing of the concrete in the compression zone. Finally, the concrete at the top of the beam was crushed, triggering the test specimen to lose its load-bearing capacity (Fig. 11). Before the test beam fractured, the component presented an intense deflection, evident signs of damage, and promising ductility.

Fig. 12 shows the damage history for the test specimen with three openings (beam P-5). Vertical cracks first emerged in the concrete below the three web openings, and then the concrete in the top of the left and right web opening cracked as the load increased. Later, the main crack extended through the beam, and a concrete crack expansion was observed under the spreader beam left support. Compared to beam P-4, beam P-5 contained fewer cracks and reached same ultimate load level. Besides, the stiffness of P-5 at yielding is 14.5 % less than P-0. The

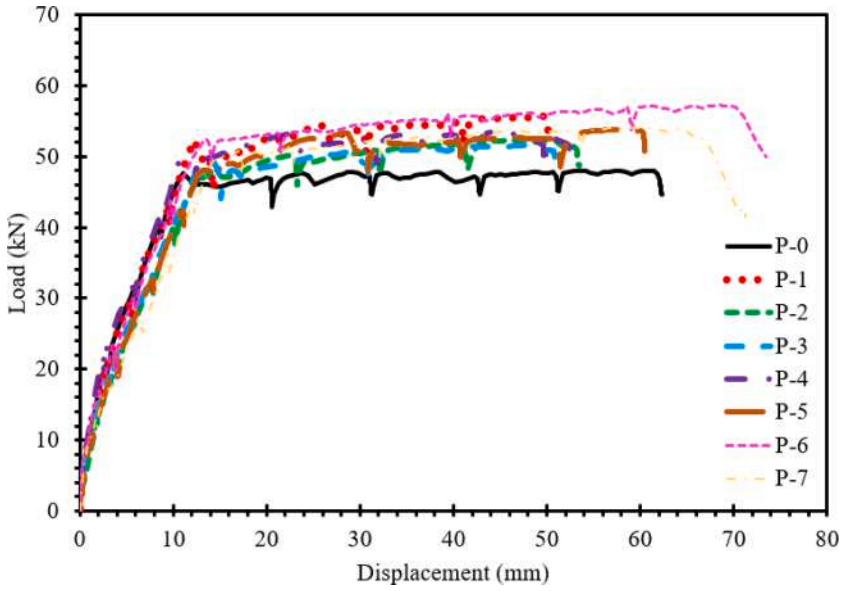

Fig 15. Comparison of specimens.

Table 2
Experimental test results.

Test specimens	P_{max} (kN)	P_u ($0.85P_{max}$) (kN)	δ_y (mm)	δ_u (mm)	Ductility Ratio (δ_u/δ_y)	Rigidityat yielding ($0.85P_{max}$)	Decrease in the Rigidity ratio of the specimens at $0.85P_{max}$	Rigidity at max. load (P_{max}) (kN/mm)	Increase in the Rigidity ratio of the specimens at P_{max}
P-0	48.00	40.80	9.00	62.29	6.92	4.53	….	0.89	….
P-1	55.68	47.32	14.50	50.18	3.46	3.26	0.28	1.12	0.26
P-2	52.33	44.48	11.78	53.44	4.53	3.77	0.17	1.04	0.17
P-3	51.57	43.84	11.25	50.89	4.52	3.89	0.14	1.08	0.21
P-4	53.48	45.46	9.64	52.63	5.45	4.71	…..	1.21	0.36
P-5	53.82	45.74	11.82	60.50	5.11	3.87	0.15	0.91	0.02
P-6	57.22	48.63	11.73	73.43	6.26	4.14	0.09	0.83	….
P-7	54.04	45.94	13.07	70.55	5.39	3.51	0.23	0.92	0.03

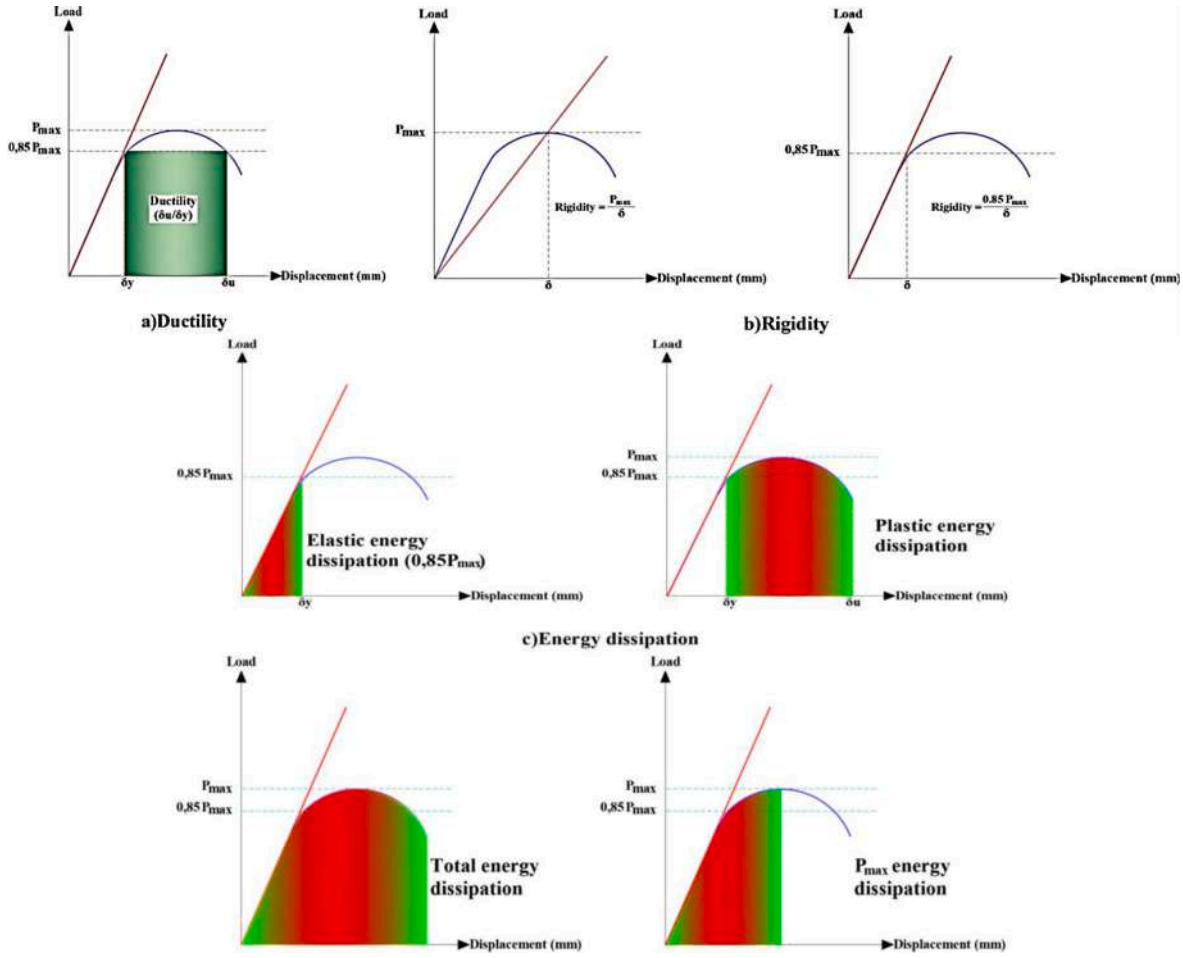

Fig. 16. Parameters considered in the evaluation of the dapped-end beams.

Table 3
Energy dissipation values of experimental test results.

Test specimens	Total energy dissipation (kj)	Energy dissipation (P_{max}) (kj)	Elastic energy dissipation ($0{,}85P_{max}$) (kj)	Plastic energydissipation (kj)
P-0	2.73	2.34	0.21	2.52
P-1	2.40	2.39	0.50	1.89
P-2	2.39	2.26	0.32	2.07
P-3	2.27	2.12	0.47	1.79
P-4	2.49	2.07	0.28	2.21
P-5	2.82	2.74	0.82	1.99
P-6	3.73	3.48	0.34	3.38
P-7	3.36	2.86	0.36	3.00

crushing damage observed in the concrete compression zone in P-4 and P-3 was not observed in P-5 because opening the gaps in three parts has ensured a more stable behavior.

P-6 specimen, in which the cracking pattern and damage analysis are shown in Fig. 13, resisted more load than other specimens. In other words, there is no loss in load-carrying capacity despite increasing the web opening ratio. With loading progress, cracks propagated at the bending region and from the bottom chords of opening towards the support. This resulted in more curvature. Subsequently, a crushing of the top layer chord of concrete has taken place. Unlike the other samples, the damage in P-5 was caused by concrete crushing in the top chord part. This may be attributed to the increase web opening. Because more weakness are available top and bottom chord in the opening zone. Besides, the stiffness of P-6 at maximum loading is 6.7 % less than P-0.

Fig. 14 shows the crack profile of the P-7 at the stage of different load levels, which are initial, elastic, yielding, and collapse. P-7 specimens have got the most significant web opening ratio compared to others. The first cracks emerged in a narrow and vertical at the mid-span of the beam. As the beam continued to deflect, flexural cracks kept propagating until 49.9 kN where a crack initiated multiway from the tensile fibers and reached the compression chord, which had caused a splitting in the concrete, and consequently, the beam collapsed as bending. The results clearly suggest that increasing the openings no significantly changes the beam's load-bearing capacity.

For all beams with 4-point bending, load versus displacement curves are plotted in Fig. 15. It is revealed that all beams had approximately the same behavior in terms of ultimate mode of failure and load–displacement characteristics. It is clear that the introduction of openings does not alter the load-carrying mechanism as long as the openings are located within the tension zone of the beam because concrete there would have cracked anyway at ultimate flexure. Consequently, the strength of the beam is not affected. Therefore, it can be concluded that locating openings with larger sizes within the bending zone may result in similar behavior as for smaller openings within zones of bending.

Table 2 shows the test results of the eight specimens in terms of critical parameters of load–displacement curves. It should be noted that the ultimate state used in Table 2 is defined as the state where the post-peak load decreases to 85 % of its peak value. In Table 2, there was no significant decrease in the maximum load carrying capacity of the reference (P-0) and purlins with different opening sizes (P-1 - P-7). In fact, increases in load carrying capacity were observed with increases in opening size. Similarly, it is important to determine the change in

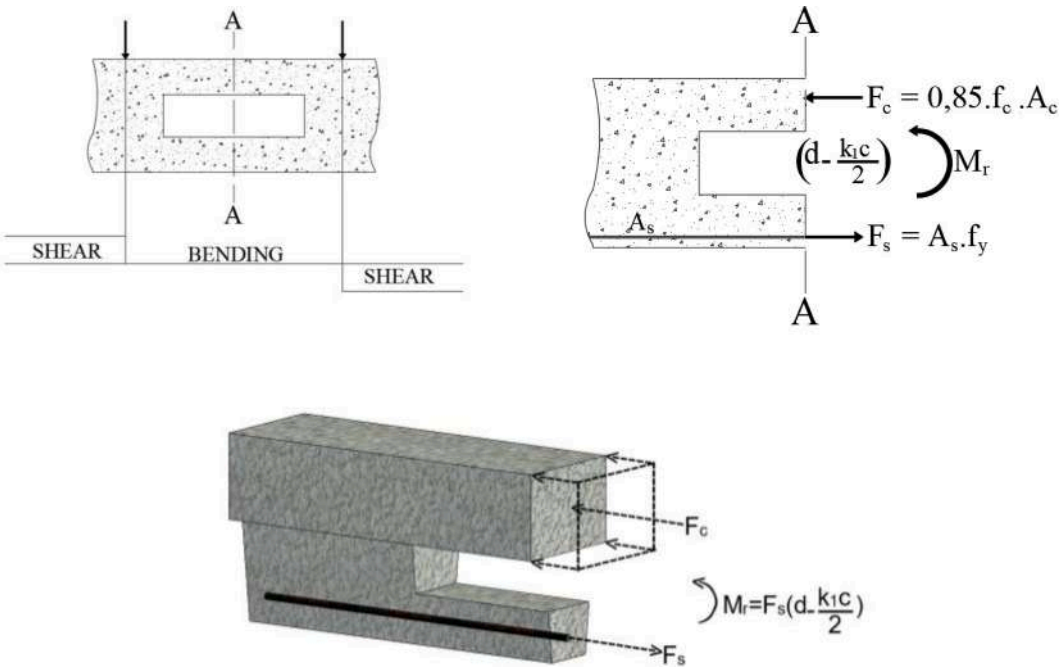

Fig. 17. Analytical calculation procedure.

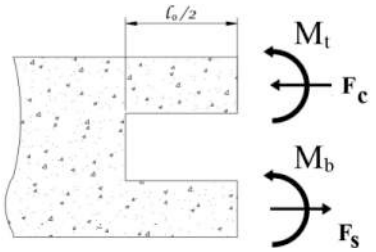

Fig. 18. Force and moment balance on the beam.

ductility, stiffness and energy dissipation capacities for each specimen. For this, the parametric values shown in Fig. 16 are calculated and given in Tables 2 and 3.

The ultimate load, rigidity, and ductility values of the specimens are compared in order to evaluate the effects of web opening ratio on beam behavior. Table 2 presents the ultimate load (P_{max}) values of the specimens and the rigidity values corresponding to P_{max} and $0.85P_{max}$. The increases in the ultimate load and rigidity of each beam with respect to the reference specimen are also indicated in the table. According to the majority of structural codes (Euroceode8) [41], the ultimate displacement corresponds to the displacement at 85 % of the ultimate load ($0.85P_{max}$) in the descending branch of the load–displacement curve. Therefore, the rigidity and energy dissipation values corresponding to 0.85Pmax in addition to the respective values corresponding to Pmax are adopted in the present study for the sake of comparing the behavior of different specimens. These values were also considered in different studies [42,43].

Furthermore, the deformation ductility ratio was calculated by dividing this ultimate displacement, i.e. the displacement at $0.85P_{max}$, to the yielding displacement. The yielding displacement represents the displacement value at which the slope of the load- displacement curve decreases significantly beyond the initial elastic linear portion (Fig. 18). The ductility ratio, total energy dissipaiton and energy dissipation at Pmax and $0.85P_{max}$ values of the specimens are tabulated in Table 2 and Table 3 together with the ratio of each value to the respective value of the related reference specimen. The fact that this ratio is around 4 ~ 5 in a ductile beam indicates that sufficient ductility condition is met. Except for the P-1 in Table 2, it is seen that sufficient ductility is provided. It should be known that if the loading could be continued without exceeding the LVDT capacity for the P-1 specimen, sufficient ductility would be achieved. Therefore, when considered for all specimens, it is clearly seen that the gaps opened to the beams are sufficient for the ductility ratios. Yield and maximum stiffness were calculated by dividing each specimen's load at yield and maximum ($0.85P_{max}$ and P_{max}) to the current displacement value. When the specimens in Table 2 are examined, it is observed that the stiffness at the yield point decreases with the increase in the opening areas. On the other hand, in the stiffness values at the maximum load, a maximum increase of 26 % was observed in P1 specimen. When this situation is compared with P-0, the increase in the opening areas caused an increase of 3–26 % in the stiffness values at the moment of maximum load. Therefore, it has been observed that the openings do not cause any loss on rigidity.

Table 3 indicates the test results regarding energy dissipation capacities. The total energy consists of elastic and plastic energy. Elastic energy is the type of energy temporarily stored in the linear elastic behavior of a system. Plastic energy is consumed after the building system's yield point (elastic limit). The total energy consumption capacities of the tested specimens were calculated from the cumulative sum of the areas under the load displacement curves. Here, at the end of the experiment, the energy values consumed at the total, maximum load, yield and plastic level were calculated. When the energy consumption capacities, which are directly proportional to the ductility, are examined, the increase in the opening ratios had a positive effect on the specimens. This situation also shows that the energy that needs to be consumed in the event of an earthquake will not be affected by the openings. Especially the increase in the plastic energy capacity consumed after the yield supports this situation.

3.2. Estimation Bending Capacity by Traditional Design Approach.

In this part of the study, purlin bending capacity was determined by traditional analysis methods before modeling with ABAQUS. Obtained results were compared with experimental data.

In the case of pure bending, if the opening or gap is in a region close to the neutral axis, there is no change in the ultimate moment capacity. In other words, the gap has no importance in the ultimate moment capacity of the beam. For this, the most important condition is that the

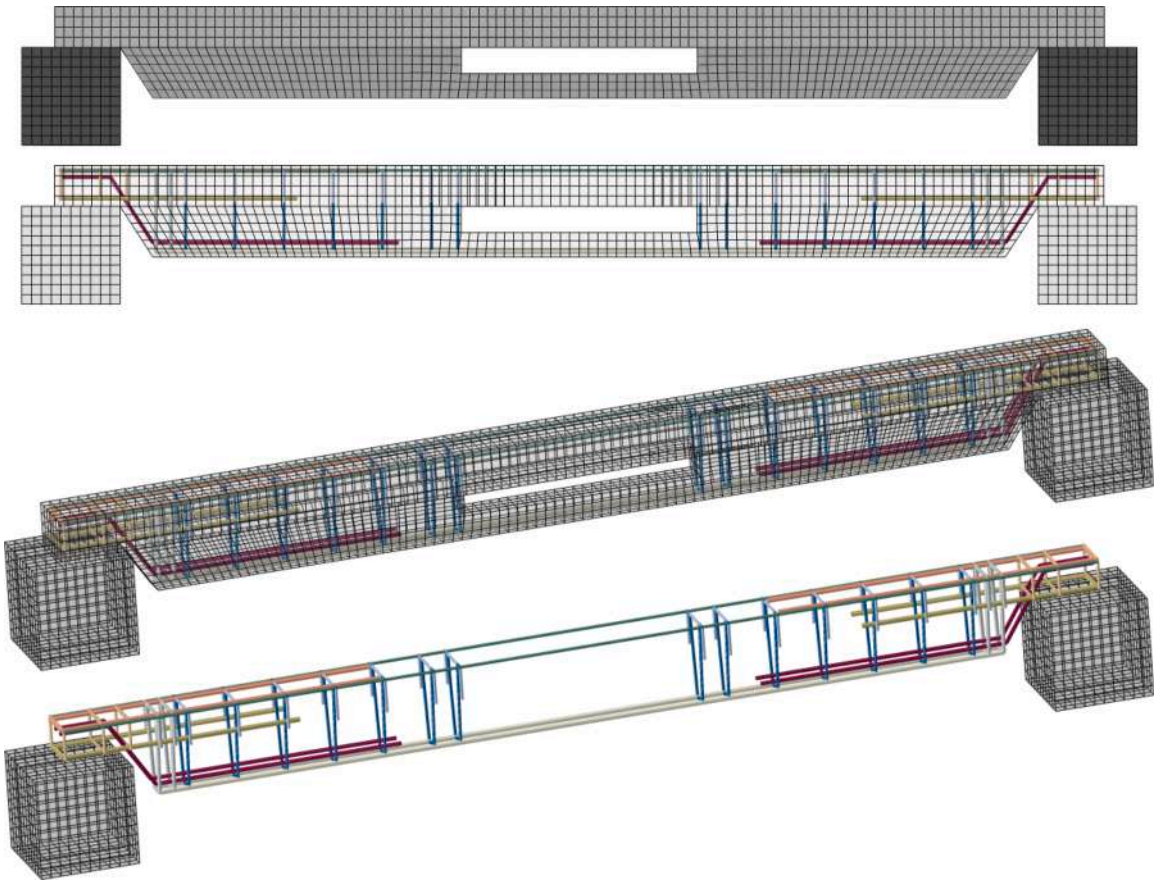

Fig. 19. Mesh configuration and reinforcement details.

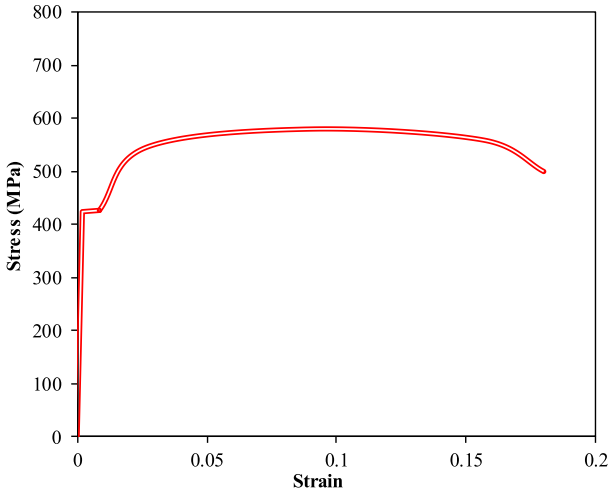

Fig. 20. Stress strain curve of steel reinforcements.

compressive stress block height does not go down to the region where the void is located. The case observed in the experiments that was conducted in this study confirms this statement. Similar results had also supported in the literature by Tan et al. [44] and Mansur et al. [45]. In pure bending, the minimum depth of the compression chord, h_c (=k_1 × c) (the depth of the stress block can be obtained by multiplying the distance from the extreme compression fiber to the neutral axis by the coefficient k_1), is greater than or equal to the depth of the ultimate compressive stress block given in Equation (1);

$$h_c < A_s x f_y/(0.85\ x\ f_c x\ b) \quad (1)$$

where A_s is the area of flexural reinforcement in beam, f_y is the yield strength of flexural reinforcement, f_c is the compressive strength of concrete and b is the beam width, A_c is the compression zone area (b × h_c). Since the upper flange of the beam considered in this study is rectangular, the b value is constant. If the compression zone had descended to the region of the body, that is, the variable cross-section, an average value ($b_{average}$) would have to be considered instead of b (Fig. 17).

The most important assumption made for the above equation to be written is that the sections that were plane before bending remain plane after bending, as put forward by Euler-Bernoulli beam theory. If the void rate is too high, this theory will lose its validity. Tan et al. [44] suggested that the amount of opening not exceeding 40 % of the total cross-section is the limit. In this study, the classical bending theory will be valid since the designed cavity height is in this order. In other words, in such a case, beam behavior may be assumed to prevail. In this case, moment carrying capacities can be found by writing the equilibrium equations for the beams tested in the experimental study. For the equilibrium equations, the forces F_c and F_s will need to be calculated as shown in Fig. 18 and then multiplied by the moment arm (j × d = d-(h_c/2))

$$M_r = A_s x\, f_y x\ (d - (h_c/2)) = A_s x\, f_y x\ j\ x\ d = 0.85\ x\ f_c x\ h_c x\ b \quad (2)$$

The load carrying capacity of the beam will also be found from the moment carrying capacity (M_r) obtained. In the equation (3), av is shear span. Applied load (V_r) since the beam was subjected to a four-point bending test in the experiments.

$$P = M_r/a_v; V_r = 2P \quad (3)$$

In this case, since it is known that the yield strength of 2ϕ10

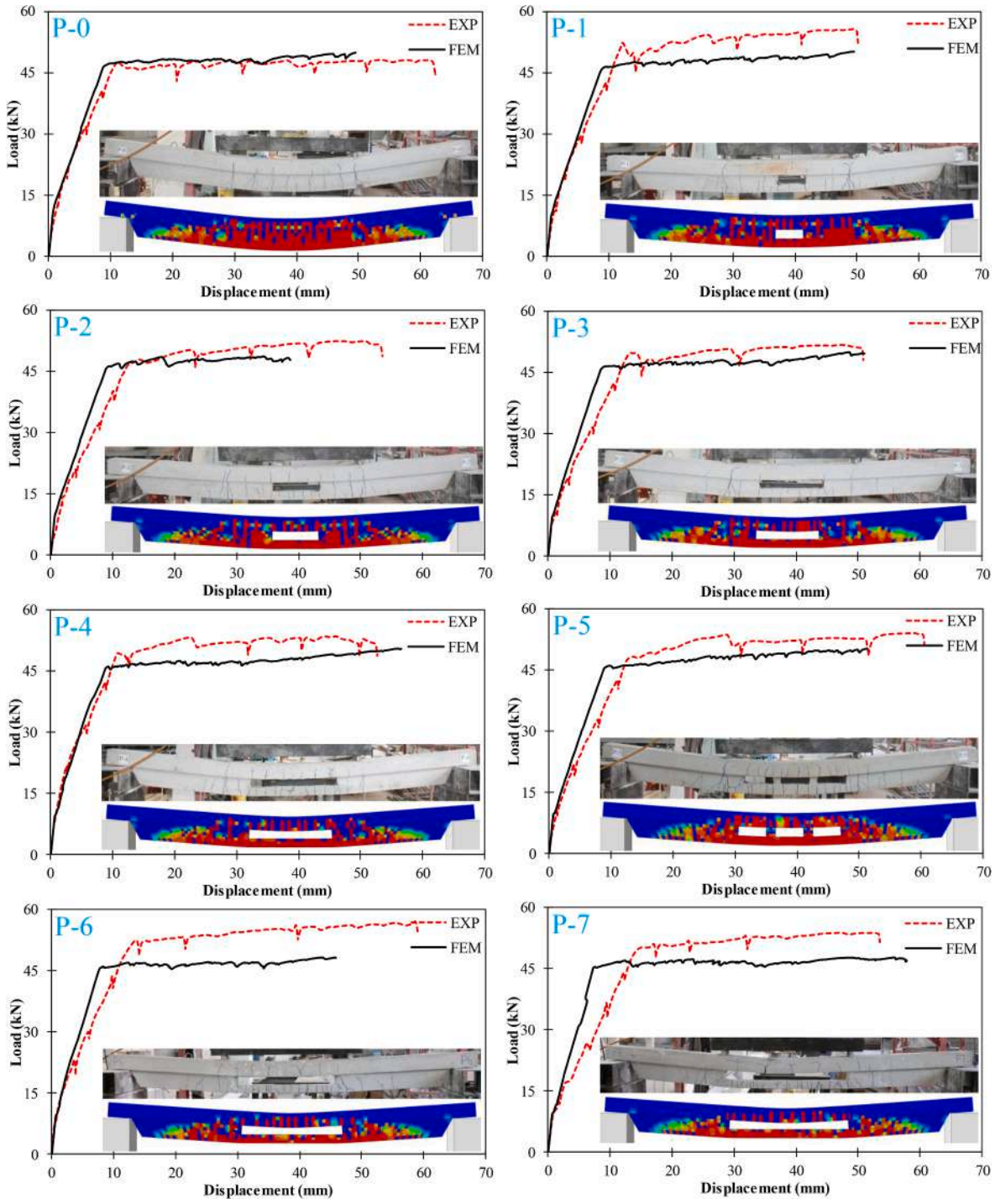

Fig. 21. Verification of the numerical model.

reinforcement in the tensile zone is f_y = 427 MPa and the ultimate strength is 550 MPa, h_c = 2.16 cm can be calculated. Since the compressive strength of the concrete used in the purlin beams is 397 kg/cm^2, the value of jxd, which is the force arm, is calculated as 26 cm. Based on this degree, the moment carrying capacity of the purlin beam, Mr, is divided by the shear span (a_v = 0.95 m) to obtain the force P and the load carrying capacity of the beam, 2P, can be calculated as 47.5kN. From the experiments described in Section 3.1, 48kN was found for P-0. In this respect, the results obtained are in good agreement with the capacity of the purlins without opening.

However, as a result of the gap formation in the purlins, hinges occurred in the upper and lower chords. As a result of the plastic hinges, there is a slight increase in the M_r moment capacity. In this case, the following Equation (4) can be written for the moment carrying capacity of beams with openings. Here M_r is the moment carrying capacity found from the above equation. M_t and M_b are the moments resulting from additional hinges in the upper and lower cords, respectively.

$$M_r + M_t + M_b = M_r' \tag{4}$$

However, the limited depth of the upper and lower chords (12.5 cm upper chord and 7.5 cm lower chord) also limits the contribution of M_t and M_b. Since the chord dimensions are the same in P-1/P-7 specimens, M_t and M_b contribution will not change. The contribution of M_t and M_b is

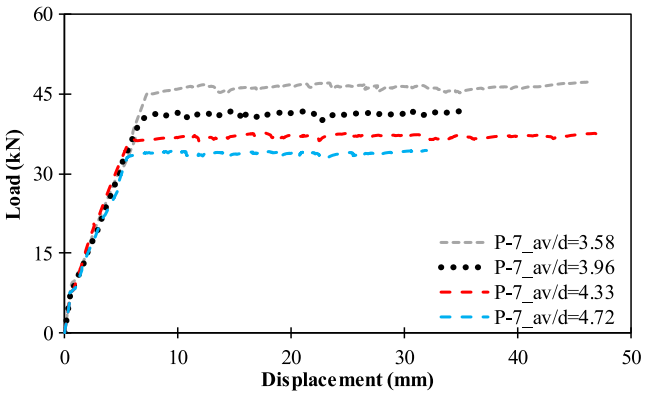

Fig. 22. Load-displacement curves depending on a_v/d ratios.

based on the contribution of reinforcement (1) (2ϕ8) and (2) (2ϕ10) given in Fig. 4, respectively. In this case, reinforcement (1) contributes 5.2 kNm and reinforcement (2) contributes 4.0 kNtm. In this case, the load carrying capacity (2P) of beams with opening can be calculated by writing Equation (5) according to M_r' value. From this, V_r value is obtained as 66.8 kN.

$$P = M_r^{'}/a_v; V_r = 2P \tag{5}$$

The fact that this value is slightly higher than the experimental values also means that damage occurred in the chords before reaching capacity (crushing of the concrete before the reinforcement yields). It is seen that the M_r' moment value obtained is independent of the opening length. This is supported by the fact that the values obtained from the purling with opening are close to each other.

4. Numerical study

4.1. Modeling assumptions

Numerical analyses were performed in ABAQUS environment. The aim of the numerical study was (i) to examine the effects of the a/d ratio and to investigate the effects of large openings which did not be studied in the experiments. Pursuant to these goals, three-dimensional numerical models were constructed. Concrete and steel supports were modeled using C3D8R elements whereas T3D2R was chosen for the reinforcements. Fig. 19 illustrates mesh configuration and the reinforcement details for P-4. The mesh size is important for accuracy of numerical modeling [46,47]. Therefore, a mesh optimization study was conducted to obtain high accuracy with optimum computational time. Mesh size of 10 mm, 20 mm and 30 mm was investigated. Decreasing mesh size to 10 mm significantly increased the computational time but a slight difference was detected on load–displacement curves. On the other hand, using mesh size as 30 mm resulted in low accuracy. Therefore, mesh size shown in Fig. 19 was determined based on the mesh-sensitive analyses.

All degrees of freedom were restrained below the steel supports. Frictional surfaces between the steel supports and purlin were defined. A friction coefficient of 0.7 between the supports and purlin was selected based on the previous studies [11,32,48]. The embedded option was utilized for interaction between concrete and reinforcements.

For modeling reinforced concrete, the concrete damaged plasticity model (CDPM) was adapted [31,49]. The dilation angle, the flow potential eccentricity, the ratio of initial biaxial compressive yield stress to initial uniaxial compressive yield stress, the ratio of the second stress invariant on the tensile meridian to that on the compressive meridian, and the viscosity parameter were defined as 31, 0.1, 1.16, 0.667 and 0.0001 respectively. These parameters were suggested by Dere [49] to obtain shear and flexural cracks. Using low value of viscosity parameter leads to accurate results and but may result in convergence problems; therefore, this parameter was used as minimum as possible. The compressive strain and stress curve is obtained from the following Eq.

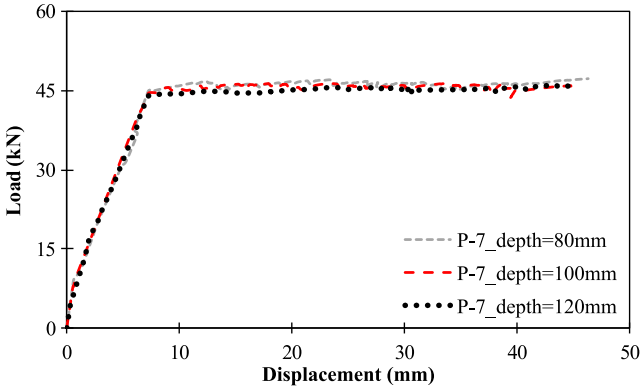

Fig. 24. Load-displacement curves depending on depth of opening.

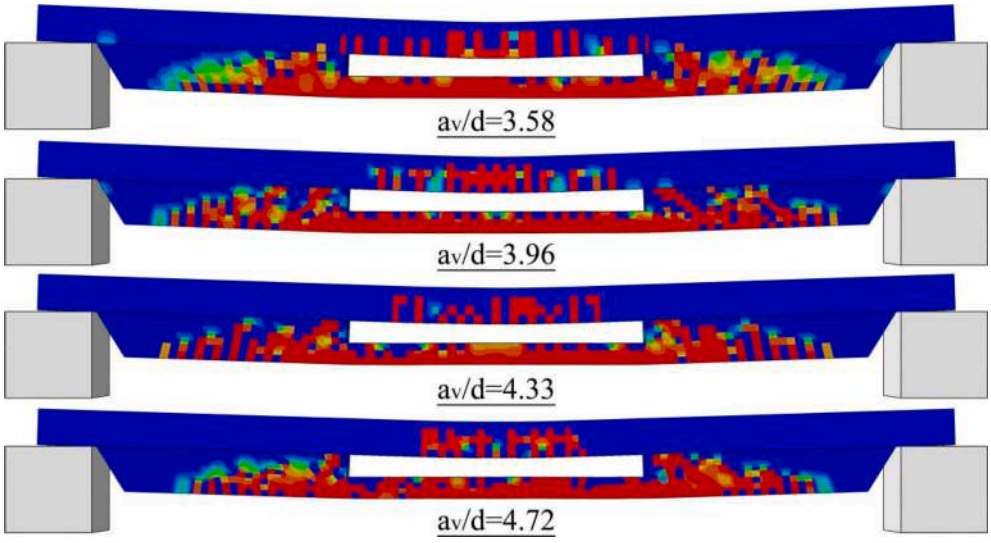

Fig. 23. Crack patterns depending on a_v/d ratios.

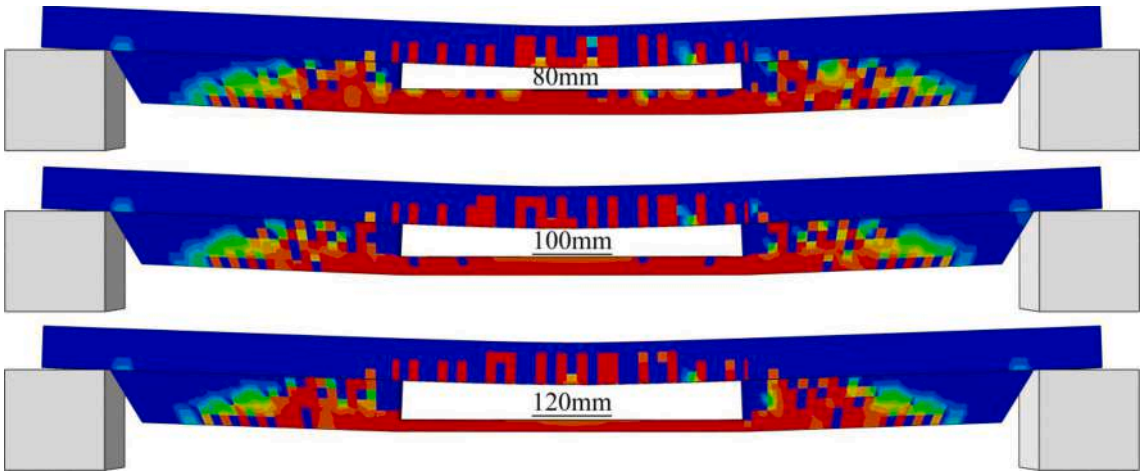

Fig. 25. Crack patterns depending on depth of opening.

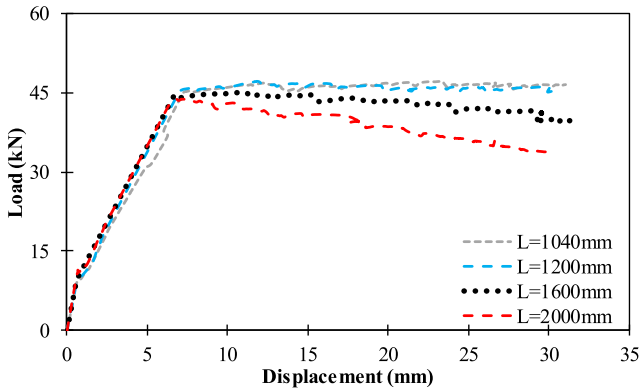

Fig. 26. Load-displacement curves depending on length of opening.

(6):

$$\frac{\sigma_c}{f_c} = \frac{n\left(\frac{\varepsilon_c}{\varepsilon_{co}}\right)}{(n-1)+\left(\frac{\varepsilon_c}{\varepsilon_{co}}\right)^n} \tag{6}$$

where σ_c is compressive stress, ε_c is a compressive strain, f_c is uniaxial compressive strength and ε_{co} is a uniaxial compressive strain. n is obtained from following Eq. (7):

$$n = 0.058 f_c + 1.0 \tag{7}$$

For tensile behavior of the concrete, the tension stiffening model was utilized based on the model proposed by Nayal and Rasheed [50]. The tensile stress and strain relationship are defined by Eq.8 and Eq.9, respectively.

$$\sigma_t' = 0.3 f_c^{(2/3)} \tag{8}$$

where

$$\varepsilon_{cr} = \frac{\sigma_t'}{E_c} \tag{9}$$

where E_c is the slope of the initial tangent of compressive stress and strain curve.

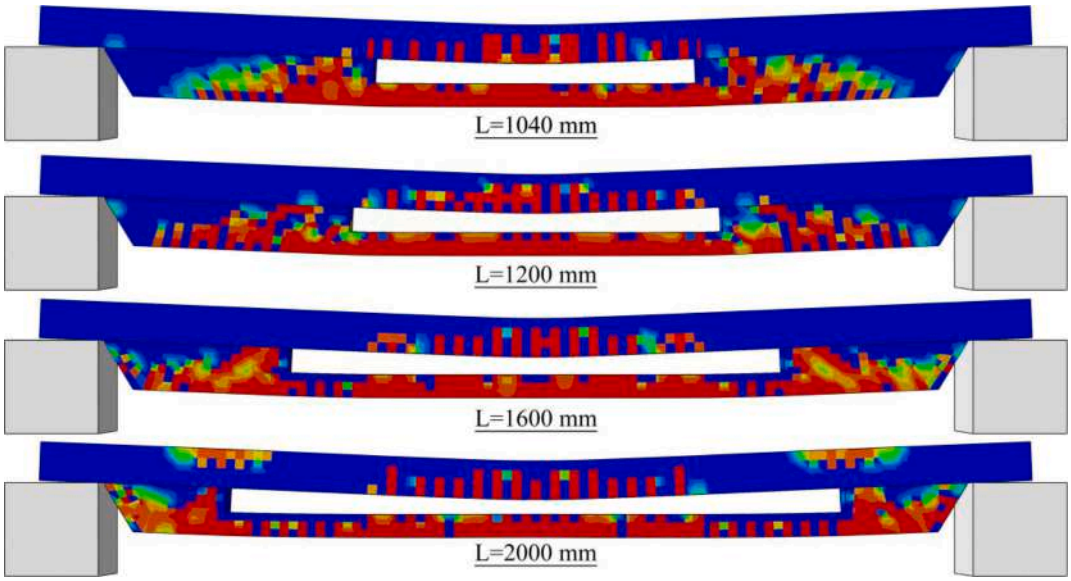

Fig. 27. Crack patterns depending on length of opening.

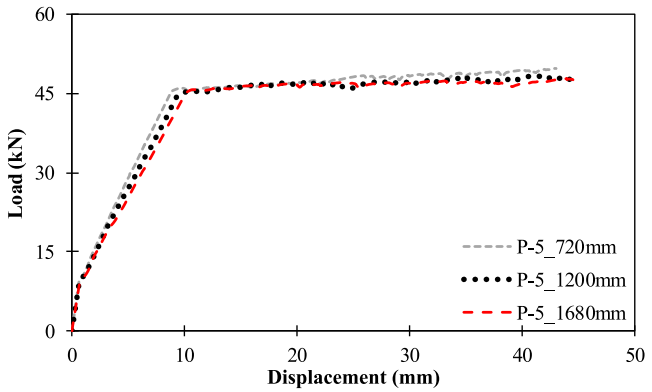

Fig. 28. Load-displacement curves depending on the number of small openings.

Two damage parameters are defined in CDPM: concrete compression damage parameter (d_c) and concrete tension damage parameter (d_t). These parameters can take values from zero to one depending on the severity of the damage. The value of 0 stands for the undamaged material while the value of 1 stands for fully damaged material. These parameters are defined in Eq. (10) and Eq. (11):

$$d_c = 1 - \frac{\sigma_c E_c^{-1}}{\varepsilon_c^{pl}(1/b_c - 1) + \sigma_c E_c^{-1}} \tag{10}$$

$$d_t = 1 - \frac{\sigma_t E_c^{-1}}{\varepsilon_t^{pl}(1/b_t - 1) + \sigma_t E_c^{-1}} \tag{11}$$

For modeling steel reinforcements, tensile tests of these bars used in the experimental study were utilized. According to tensile test results, average of 427 MPa was obtained. The stress–strain curve utilized in the numerical models is shown in Fig. 20.

This study is part of comprehensive experimental and numerical study on prefabricated purlins [31,32,40,51]. The authors carried out several parametric numerical studies on these purlins and the parameters utilized in this study were previously verified in these studies. Therefore, modeling assumptions used in these studies [31,32,40,51] were adopted.

4.2. Verification of numerical model

In order to verify the assumptions in the numerical models, the experimental findings in terms of load–displacement curves and cracking patterns were utilized for this purpose. Fig. 21 demonstrates the comparison of the experimental and numerical results. The results indicate that the numerical models are able to capture the behavior of the experimented specimens. The finite element models slightly resulted in stiffer behavior. The reason for high stiffness can be attributed to that the numerical models can not model micro-cracks and perfect bonding between the reinforcements and concrete. Moreover, the reason for difference between the capacities of numerical and experimental findings can be attributed the material modeling of concrete and steel reinforcement. There may be slight difference in steel reinforcements and concrete during the production and also material models can be exact with the materials utilized in the experiments.

4.3. Parametric numerical study

Firstly, the effects of a_v/d were investigated in Specimen P-7 since Specimen P-7 is the most critical section. For this aim, the a_v/d ratios of 3.58, 3.96, 4.33 and 4.72 were investigated by keeping all experimental parameters are constant. Fig. 22 demonstrates load–displacement curves for Specimen P-7 depending on different a_v/d ratios. The results show that no strength degradation is observed due to increasing a_v/d ratios. This indicates that the purlins with openings can perform successfully regardless of a_v/d ratios. Furthermore, Fig. 23 illustrates the cracking patterns occurred on the models. As the ratio of a_v/d increases, the occurrence of the shear cracking are less pronounced. The cracking around the openings is very similar.

The effects of the depth of opening were examined in Specimens P-7 due to the aforementioned reason. The depth of 80 mm, 100 mm and 120 mm was selected by keeping all experimental parameters are constant for this purpose. Fig. 24 shows the load–displacement curves of these models. It is seen that a very slight effect on the behavior is observed. Moreover, the crack patterns observed in the models are depicted in Fig. 25. Although all models demonstrated similar performance, increasing depth of the opening up to longitudinal reinforcements should not be performed. For instance, when the depth of opening is 120 mm, a total of concrete cover (20 mm + 20 mm) is 40 mm. When inadequate workmanship is performed, a catastrophic effect may arise.

The effects of the length of opening were examined using three different lengths. The opening lengths of 1200 mm, 1600 mm and 2000 mm were selected by keeping all experimental parameters are constant. The opening length was 1040 mm in the experimented Specimen P-7. Load-displacement curves of these models are shown in Fig. 26. Increasing the opening length from 1040 mm to 1200 mm resulted no adverse effect. However, when the opening lengths were 1600 mm and 2000 mm, significant decreases in the capacity were observed after reaching the maximum load level. Fig. 27 demonstrates the cracking pattern observed in the models. It is seen that the bottom chord of the models with 1600 mm and 2000 mm moved upward, which indicates

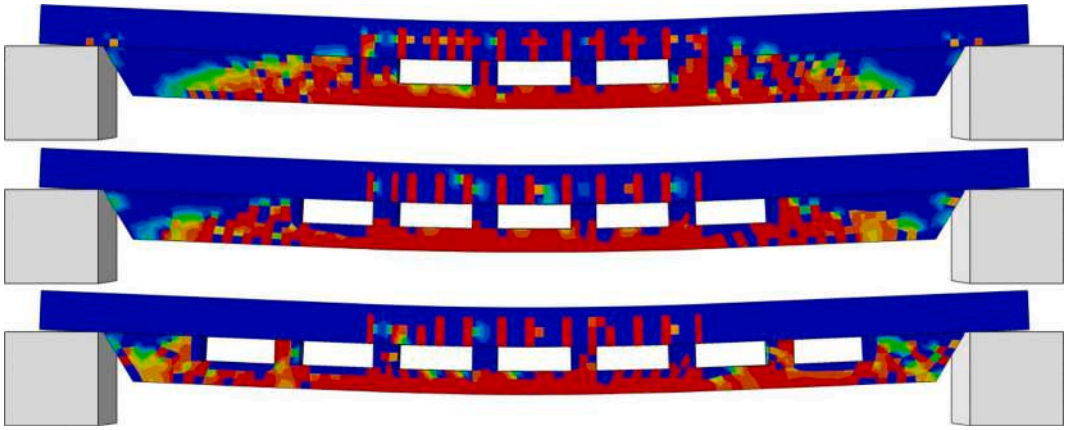

Fig. 29. Crack patterns depending on the number of small openings.

that bottom and upward chords act indepently.

In order to mitigate the problems observed in the models with large openings, the approach utilized in the experimented Specimen P-5 adopted. Instead of using large openings, small openings with high numbers were utilized. In this way, top and bottom chords act together. In Specimen P-5, three small openings of 240 mm (total of 720 mm) were utilized. In order to further increase the total length of the opening, the models with 5 (total of 1200 mm) and 7 (total of 1680 mm) small openings were analyzed by keeping all experimental parameters are constant. It is seen in Fig. 28 that no strength degradation was observed in any models. This reveals that when the proper interaction between top and bottom chords was preserved, no strength degradation was utilized. Small openings may provide this opportunity. The displacements observed in Fig. 29 also prove this concept.

5. Results

In this study, different web openings were applied to understand the bending behavior of dapped-end RC purlin beams using experimental and analytical approaches. Eight full scale purlin beams were tested under four point loading. The following results were obtained from from experimental part:

- The increase in the opening area did not provide a significant effect on the capacity. This can be explained by the fact that the openings are in the bending region.
- All the specimens failed in a flexural mode associated with the web openings. The P-5 specimen improved the efficiency of web openings.
- Compared with the reference P-0 beam, the bending capacity of the dapped-end beams with web openings were increased by between 7.4 % and 19.2 %, respectively. The bending capacity and ultimate deflection of the dapped-end beams did not lose as the web opening ratio increased.
- The internal stress of the beams was redistributed after bending cracking. The failure mechanism differed from that of the reference beam P-0 for the web opening beams under sustained load. In practical applications, to improve the structural behaviors and economical gain of dapped-end beams, the RC beams can be used with web opening and do not require any strengthening.
- P-5 specimen reveals a more stable structure compared to other specimens. Exceptionally, proper interaction between top and bottom chords was preserved. Therefore, it is recommended to create openings similar to the P-5 specimen.

After verifying experimental results with the aid of ABAQUS, a parametric study was performed. ABAQUS models were utilized to predict the bending capacity of dapped-end beams with different web opening parameters. In the model, the influences of the bending damage degree and sustaining load level could be considered. The following results were obtained from numerical part:

- In parametric studies performed on the specimens with the largest opening ratio, it has been observed that an increase in a_v/d ratio causes a decrease in load carrying capacity even if there is no change in rigidity.
- No effect of the gap height was observed if openings are away from the upper and lower reinforcements at least as much as the concrete cover margin.
- If the gap length to total length ratio exceeds 0.375, the strength of the purlin decreased significantly after the reinforcement yields. This showed that the strength would not be lost if the gap came closer to the purlin supports by more than 2xh. However, if the opening is not made in one piece, but in parts (3 × 24, 5 × 24 and 7 × 24 cm), a significant effect of the total opening length on the purlin mechanical behavior was not observed.

6. Conclusion and Final Remarks

In the light of the results obtained the behavior of purlin beams having different openings (gaps) studies have been reached by experimentally and numerically. The most important result obtained from this study, especially in reinforced concrete prefabricated structures, which are frequently preferred in industrial buildings, limited opening (especially opening length / purlin length ratio is lower than 0.375) in purlin's bending zones will not have a negative effect on the bearing capacity, but it will cause a considerable decrease in the use of concrete materials. This can be explained by the fact that the openings are in the bending region. Also the numerical findings showed that increasing shear span to depth ratio (a_v/d) ratio did not change rigidity but decreased the load capacity. However, no effect was observed on the opening height provided that it is at least as far away from the upper and lower longitudinal reinforcements bars as the concrete-cover margin. On the other hand, increasing opening/purlin length (higher than 0.375) reduces the load carrying capacity. However, segmented openings (multiple openings instead of single whole openings) did not reduce capacity even if total opening/purlin length was 0.525. In addition, no additional reinforcement arrangement was made around the opening borders. Moreover, among the opening length stirrups were not used. It is obvious that there factors will also cause a decrease in the cost of the reinforcement. Therefore, all these obtained results have encouraging clues in purlin design for prefabricated building manufacturers. In practice, it is obvious that the purlins will not bend from four points as in the experiments in this study, and that the purlins will be under the effect of shear force as well as the bending moment. However, since the certainty of the shear will not have such a damaging effect as bending after a critical region, it is seen that the gaps to be opened after a certain distance (2.h) to the supports will be beneficial in this sense.

Declaration of Competing Interest

The authors declare that they have no known competing financial interests or personal relationships that could have appeared to influence the work reported in this paper.

Acknowledgements

This study was supported by Konya Technical University Research Projects Coordination Unit (Project Number: 211004018).Authors also would like to thank Yardımcı Prefabricated Building Components Inc.for helping producing purlins.

References

[1] Vidjeapriya R, Jaya KP. Experimental Study on Two Simple Mechanical Precast Beam-Column Connections under Reverse Cyclic Loading. J Perform Constr Facil 2013;27:402–14.
[2] Guerrero H, Rodriguez V, Escobar JA, Alcocer SM, Bennetts F, Suarez M. Experimental tests of precast reinforced concrete beam-column connections. Soil Dyn Earthq Eng 2019;125:105743.
[3] Gou S, Ding R, Fan J, Nie X, Zhang J. Seismic performance of a novel precast concrete beam-column connection using low-shrinkage engineered cementitious composites. Constr Build Mater 2018;192:643–56.
[4] Guo X, Gao S, Wang L, Bui TN. Bearing capacity of embedded channel-shaped steel connections at precast concrete beam end. Eng Struct 2018;175:177–90.
[5] Huang W, Hu G, Zhang J. Experimental study on the seismic performance of new precast concrete beam-column joints with replaceable connection. Structures 2022;35:856–72.
[6] Ahmed S, Arocho I. Analysis of cost comparison and effects of change orders during construction: Study of a mass timber and a concrete building project. J Build Eng 2021;33:101856.
[7] Sadri H, Pourbagheri P, Yitmen I. Towards the implications of Boverket's climate declaration act for sustainability indices in the Swedish construction industry. Build Environ 2022;207:108446.
[8] Basaran B, Kalkan I, Aksoylu C, Özkılıç YO, Sabri MMS. Effects of Waste Powder, Fine and Coarse Marble Aggregates on Concrete Compressive Strength. 2022;14:14388.

[9] Beskopylny AN, Shcherban' EM, Stel'makh SA, Meskhi B, Shilov AA, Varavka V et al. Composition Component Influence on Concrete Properties with the Additive of Rubber Tree Seed Shells. 2022;12:11744.
[10] Qaidi S, Najm HM, Abed SM, Özkılıç YO, Al Dughaishi H, Alosta M et al. Concrete Containing Waste Glass as an Environmentally Friendly Aggregate: A Review on Fresh and Mechanical Characteristics. 2022;15:6222.
[11] Shcherban' EM, Stel'makh SA, Beskopylny AN, Mailyan LR, Meskhi B, Shilov AA et al. Normal-Weight Concrete with Improved Stress–Strain Characteristics Reinforced with Dispersed Coconut Fibers. 2022;12:11734.
[12] Zeybek Ö, Özkılıç YO, Çelik Aİ, Deifalla AF, Ahmad M, Sabri Sabri MM. Performance evaluation of fiber-reinforced concrete produced with steel fibers extracted from waste tire. 2022;9.
[13] Zeybek Ö, Özkılıç YO, Karalar M, Çelik Aİ, Qaidi S, Ahmad J et al. Influence of Replacing Cement with Waste Glass on Mechanical Properties of Concrete. 2022; 15:7513.
[14] Commission E. The European green deal Eur Comm 2019;53:24.
[15] Assembly G. Resolution adopted by the General Assembly on 27 July 2012. United Nations: Norfolk, VA, USA. 2012.
[16] Çelik Aİ, Özkılıç YO, Zeybek Ö, Karalar M, Qaidi S, Ahmad J et al. Mechanical Behavior of Crushed Waste Glass as Replacement of Aggregates. 2022;15:8093.
[17] Çelik Aİ, Özkılıç YO, Zeybek Ö, Özdöner N, Tayeh BA. Performance Assessment of Fiber-Reinforced Concrete Produced with Waste Lathe Fibers. 2022;14:11817.
[18] Aykac B, Kalkan I, Aykac S, Egriboz YE. Flexural behavior of RC beams with regular square or circular web openings. Eng Struct 2013;56:2165–74.
[19] Balaji G, Vetturayasudharsanan R. Experimental investigation on flexural behaviour of RC hollow beams. Mater Today: Proc 2020;21:351–6.
[20] Amin HM, Agarwal V, Aziz OQ. Effect of opening size and location on the shear strength behavior of RC deep beams without web reinforcement. International Journal of Innovative Technology and Exploring Engineering 2013;3:28–30.
[21] Eun HC, Lee YH, Chung HS, Yang KH. On the shear strength of reinforced concrete deep beam with web opening. Struct Design Tall Spec Build 2006;15:445–66.
[22] Guan H. Effect of sizes and positions of web openings on strut-and-tie models of deep beams. Adv Struct Eng 2005;8:69–84.
[23] Tseng C-C, Hwang S-J, Lu W-Y. Shear strength prediction of reinforced concrete deep beams with web openings. ACI Struct J 2017;114:1569–79.
[24] Osman BH, Wu E, Ji B, Abdulhameed SS. Shear behavior of reinforced concrete (RC) beams with circular web openings without additional shear reinforcement. KSCE J Civ Eng 2017;21:296–306.
[25] Elsanadedy HM, Al-Salloum YA, Almusallam TH, Alshenawy AO, Abbas H. Experimental and numerical study on FRP-upgraded RC beams with large rectangular web openings in shear zones. Constr Build Mater 2019;194:322–43.
[26] Abdalla HA, Torkey AM, Haggag HA, Abu-Amira AF. Design against cracking at openings in reinforced concrete beams strengthened with composite sheets. Compos Struct 2003;60:197–204.
[27] al-Attar T, Hassan Q, Mejbel S, Dawood H. The role of cover and rebar characteristics on load-slip behavior of reinforced concrete members in compression. MATEC Web of Conferences: EDP Sciences; 2018. p. 04017.
[28] Barros JAO, Dias SJE. Near surface mounted CFRP laminates for shear strengthening of concrete beams. Cem Concr Compos 2006;28:276–92.
[29] Aksoylu C, Yazman Ş, Özkılıç YO, Gemi L, Arslan MH. Experimental analysis of reinforced concrete shear deficient beams with circular web openings strengthened by CFRP composite. Compos Struct 2020;249:112561.
[30] Gemi L, Aksoylu C, Yazman Ş, Özkılıç YO, Arslan MH. Experimental investigation of shear capacity and damage analysis of thinned end prefabricated concrete purlins strengthened by CFRP composite. Compos Struct 2019;229:111399.
[31] Aksoylu C, Özkılıç YO, Yazman Ş, Gemi L, Arslan MH. Experimental and Numerical Investigation of Load Bearing Capacity of Thinned End Precast Purlin Beams and Solution Proposals. Teknik Dergi 2021.
[32] Aksoylu C, Özkılıç YO, Arslan MH. Damages on prefabricated concrete dapped-end purlins due to snow loads and a novel reinforcement detail. Eng Struct 2020;225: 111225.
[33] El Ame F, Mwero JN, Kabubo CK. Openings Effect on the Performance of Reinforced Concrete Beams Loaded in Bending and Shear. Eng Technol Appl Sci Res 2020;10:5352–67.
[34] Agag F, Ahmad SS, Sallam H-E-D-M. Experimental assessment of different strengthening techniques for opening in reinforced concrete beams. Frattura ed Integrità Strutturale 2022;16:549–65.
[35] El-Sisi AA, El-Emam HM, El-Kholy A-E-M-I, Ahmad SS, Sallam HM, Salim HA. Structural Behavior of RC Beams Containing Unreinforced Drilled Openings with and without CFRP Strengthening. Polymers 2022;14:2034.
[36] Kalkan İ, Kahraman E, Başaran B. Farklı Donatı Oranlarına Sahip Düzenli Kare Boşluklu Betonarme Kirişlerin Eğilme Davranışları. Journal of the Institute of Science and Technology 2019;9:1417–30.
[37] Aykac B, Aykac S, Kalkan I, Dundar B, Can H. Flexural Behavior and Strength of Reinforced Concrete Beams with Multiple Transverse Openings. ACI Struct J 2014; 111.
[38] TS9967. Design Construction and Erection Methods for Precast Reinforced and Prestressed Concrete Elements Structures and Buildings. 1992.
[39] Barka G, Ataköy H, Yüksel E. Beton Prefabrikasyon El Kitabı, Tasarım, Üretim ve Montaj Esasları. Ankara: Türkiye Prefabrik Birliği; 2018.
[40] Özkılıç YO, Yazman Ş, Aksoylu C, Arslan MH, Gemi L. Numerical investigation of the parameters influencing the behavior of dapped end prefabricated concrete purlins with and without CFRP strengthening. Constr Build Mater 2021;275: 122173.
[41] Code P. Eurocode 8: Design of structures for earthquake resistance-part 1: general rules, seismic actions and rules for buildings. Brussels: European Committee for Standardization; 2005.
[42] Zhang Q, Yu Q, Guan J, Wu Z. Seismic behavior of confined RC column-composite beam joints. Transactions of Tianjin University 2014;20:174–81.
[43] An D, Qu T. Experimental Study to Strengthen Two-story Brick Buildings with Precast Floor Slabs. International Journal of Simulation-Systems. Sci Technol 2016: 17.
[44] Tan K-H, Mansur M, Wei W. Design of reinforced concrete beams with circular openings. Structural Journal 2001;98:407–15.
[45] Mansur M, Tan K-H, Wei W. Effects of creating an opening in existing beams. Structural Journal 1999;96:899–905.
[46] Sharaky IA, Reda RM, Ghanem M, Seleem MH, Sallam HEM. Experimental and numerical study of RC beams strengthened with bottom and side NSM GFRP bars having different end conditions. Constr Build Mater 2017;149:882–903.
[47] Sharaky IA, Baena M, Barris C, Sallam HEM, Torres L. Effect of axial stiffness of NSM FRP reinforcement and concrete cover confinement on flexural behaviour of strengthened RC beams: Experimental and numerical study. Eng Struct 2018;173: 987–1001.
[48] Özkılıç YO, Aksoylu C, Arslan MH. Numerical evaluation of effects of shear span, stirrup spacing and angle of stirrup on reinforced concrete beam behaviour. Structural Engineering and Mechanics, An Int'l Journal 2021;79:309–26.
[49] Dere Y. Assessing a retrofitting method for existing RC buildings with low seismic capacity in Turkey. J Perform Constr Facil 2017;31:04016098.
[50] Nayal R, Rasheed HA. Tension stiffening model for concrete beams reinforced with steel and FRP bars. J Mater Civ Eng 2006;18:831–41.
[51] Özkılıç YO, Aksoylu C, Arslan MH. Experimental and numerical investigations of steel fiber reinforced concrete dapped-end purlins. J Build Eng 2021;36:102119.
[52] Fayed S, Madenci E, Özkılıç YO. Flexural behavior of RC beams with an abrupt change in depth: experimental work. Buildings 2022;12:2176.
[53] Aksoylu C, Özkılıç YO, Arslan MH. Experimental and numerical investigation of shear strength at dapped end beams having different shear span and recess corner length. Structures 2022;48:79–90.
[54] Çeledir E. Behavior of prefabricated reinforced concrete purlins having web openings under vertical loads [Master's thesis]. Konya Technical University; 2022.